Design of a Robotic Laparoscopic Tool with Modular Actuation

Kai Xu[1(✉)], Huichao Zhang[2], Jiangran Zhao[2], and Zhengchen Dai[2]

[1] The State Key Laboratory of Mechanical System and Vibration, Shanghai Jiao Tong University, Shanghai 200240, China
k.xu@sjtu.edu.cn

[2] The RII Lab (Lab of Robotics Innovation and Intervention), UM-SJTU Joint Institute, Shanghai Jiao Tong University, Shanghai 200240, China
{zhc_zju_sjtu, zjr318, zhengchen.dai}@sjtu.edu.cn

Abstract. This paper presents the development of a modular robotic laparoscopic tool for MIS (Minimally Invasive Surgery). A dual continuum mechanism is utilized in the tool design to ensure reliability as well as achieve enhanced distal dexterity, increased payload capability and actuation modularity under a simple construction. Via kinematics modeling, the laparoscopic tool could be maneuvered by a Denso manipulator to perform typical laparoscopic tasks and possesses the desired functionalities for MIS. Advantages of the implemented dual continuum mechanism lead to the performances of this attempt. Motivated by the commercial success of the da Vinci surgical system, this paper presents an alternative design to realize robotic laparoscopic surgeries, which could lead to possible future commercialization opportunities.

Keywords: Continuum mechanism · Dexterous wrist · Laparoscopic tools · Medical robotics · Surgical instruments

1 Introduction

Open surgery has been mostly replaced by MIS (Minimally Invasive Surgery) in treatments for various pathological conditions, due to the improved surgical outcomes, such as lower pain, reduced postoperative complications, and shorter hospital stay [1].

Although multi-port MIS is beneficial, manipulation of the manual tools could be challenging and exhausting, due to the lack of distal dexterity and the inversed tool-maneuvering motions. Numerous robotic systems were hence developed to assist surgeons in laparoscopic MIS for enhanced dexterity, higher motion precision, augmented tactile sensing, better ergonomics, etc. [2].

Among the existing surgical robotic systems, the da Vinci system has clinically enabled a wide spectrum of MIS procedures and dominates the market for laparoscopic surgical robots [3, 4]. Treating this system as a benchmark, the related researches primarily focus on improving (i) the tool distal dexterity [5, 6], (ii) the tactile sensing capability [7–9], and (iii) the system modularity and design compactness [10, 11]. The aforementioned systems and designs by no means exhausted all alternative design

Y. Huang et al. (Eds.): ICIRA 2017, Part II, LNAI 10463, pp. 298–310, 2017.
DOI: 10.1007/978-3-319-65292-4_26

approaches. The SMARLT (Strengthened Modularly Actuated Robotic Laparoscopic Tool) was hence developed as shown in Fig. 1, aiming at realizing robotic multi-port laparoscopic surgeries with several performance enhancements. The SMARLT tool consists of an exchangeable effector and an actuation unit.

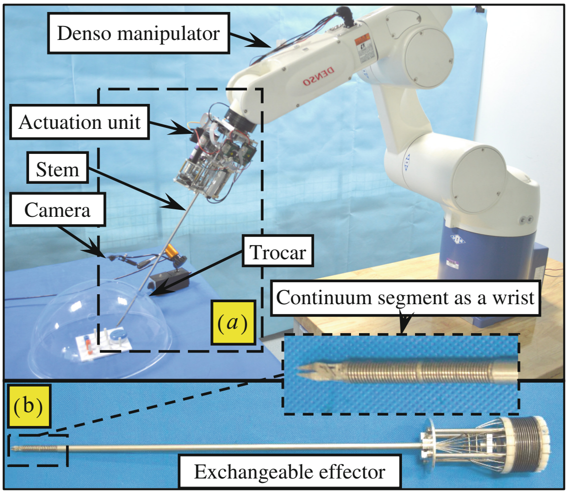

Fig. 1. The SMARLT mounted on a Denso manipulator: (a) the SMARLT tool that consists of the exchangeable effector and the actuation unit, and (b) the exchangeable effector

The SMARLT tool possesses two actuators for the wrist bending and one more actuator for the gripper. It can be attached to and maneuvered by a manipulator (e.g., the Denso manipulator in Fig. 1) for abdominal deployment through a trocar. The Denso manipulator acts as a programmable RCM (Remote Center of Motion) mechanism which positions and orients the SMARLT tool with respect to the trocar (namely, the skin incision point) in order to minimize possible tear to patient's abdominal wall. A comprehensive review of RCM mechanisms could be found in [12], while new designs were also proposed recently [13, 14].

Major contributions of this paper lie on (i) the SMARLT tool design using the concept of a dual continuum mechanism for actuation modularity and enhanced capabilities, and (ii) the analytical kinematics framework for the use of the SMARLT or similar tools with a generic manipulator under the motion constrains stemmed from the incision point. Existing results on the constrained-motion kinematics [15, 16] cannot be readily used since they don't directly include analytical formulation of the distal wrist motions. Minor contributions mainly include a compact actuation assembly design for driving the exchangeable effector.

This paper is organized as follows. With the design objectives and overview of the SMARLT tool summarized in Sect. 2, Sect. 3 describes the SMARLT design and the system components in detail. Section 4 presents a kinematics framework for the use of the SMARLT tool with a generic manipulator. Conclusions and future work are summarized in Sect. 5.

2 Design Objectives and Overview

The SMARLT tool was developed to facilitate multi-port robotic laparoscopic surgeries. It shall be attached to a manipulator so that the tool-manipulator system, shown in Fig. 1, could be tele-operated to perform surgical tasks.

Comparing to the aforementioned existing robotic systems, the SMARLT aims at realizing a few improvements. The design objectives are formulated as follows.

- The tool shall possess a wrist with small bending radius and at least two DoFs (Degrees of Freedom) for distal dexterity enhancement.
- The end effector of the tool could be changed during a surgery for different tasks and could be detached for sterilization.
- The tool could be deployed through a trocar with diameter less than 8 mm.
- Payload capability of the tool should be at least 300 g, according to the studies that the suture tension of a hand tie is less than 3 N [17, 18] and the tissue manipulation force ranges from 1.3 N to 3.5 N [19].

With the design objectives, the SMARLT tool is hence designed and constructed as in Fig. 1(a). It consists of an exchangeable effector and an actuation unit.

The exchangeable effector possesses a continuum segment as a distal wrist with a 2-DoF bending motion capability. It could be equipped with different distal surgical end effectors (e.g. gripper, scissors, cautery spatula, etc.). Different effectors (including the surgical end effector, the continuum segment, the stem, etc.) could be changed during a procedure. The effector is purely mechanical and it could be easily sterilized. The current design has a stem with a length of 400 mm and a diameter of 7 mm. The diameter is determined due to the availability of a critical component.

The actuation unit mainly includes three sets of servomotors and related actuation assemblies for driving the distal wrist and the gripper.

System descriptions of the SMARLT tool as well as the setup of the tool-manipulator system are detailed in Sect. 3. The derived kinematics is reported in Sect. 4. This kinematics framework could be applied to use the SMARLT or similar tools with a manipulator in tele-operated surgical tasks.

3 System Descriptions

The SMARLT is deployed and maneuvered by a Denso manipulator for surgical tasks in laparoscopic procedures. The SMARLT tool consists of an exchangeable effector and an actuation unit as shown in Fig. 1(a). Component descriptions of the exchangeable effector and the actuation unit are presented in Sect. 3.1 and Sect. 3.2 respectively. Controller architecture of the SMARLT tool, which allows its integrated control of Denso manipulator for teleoperation, is presented in Sect. 3.3.

3.1 Exchangeable Effector with a Continuum Wrist

The exchangeable effector shown in Fig. 1(b) is depicted in Fig. 2. It utilizes the concept of a dual continuum mechanism which is firstly proposed in [20]. The exchangeable effector consists of a gripper, a distal continuum segment, a stem, guiding cannulae, and a proximal continuum segment, as shown in Fig. 2. Both the distal and the proximal segments are structurally similar to the one shown in Fig. 5(b).

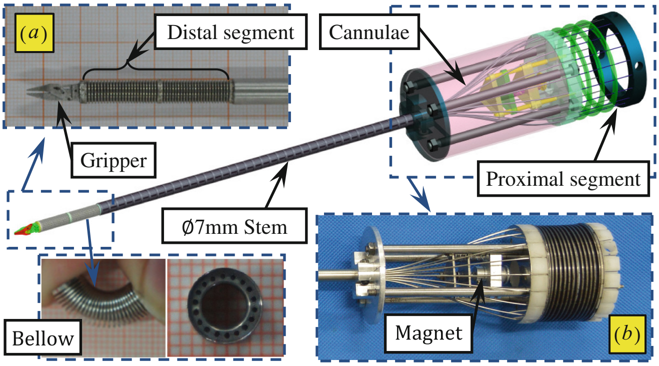

Fig. 2. The exchangeable effector of the SMARLT tool: (a) the distal segment as a wrist, and (b) the proximal segment with the gripper actuation

The segment in Fig. 5(b) consists of a base ring, several spacer rings, an end ring, and several backbones. The backbones are made from super-elastic nitinol rods. They are called backbones instead of tendons since they can be pushed and pulled while the tendons may only be pulled. Pushing and pulling these backbones bends the segment.

In the exchangeable effector shown in Fig. 2, both ends of a backbone are attached to the end rings of the distal and the proximal segments respectively, routing through the distal segment, the stem, the guiding cannulae and the proximal segment. The arrangement of the backbones in the distal segment is similar and scaled to that in the proximal segment. Hence, bending of the proximal segment always bends the distal segment in the opposite direction. This distal-proximal structure is referred to as a *dual continuum mechanism*.

Strength of the segment is affected by the diameter and the number of the backbones. In order to achieve a segment with higher payload capabilities and small bending radius, more and thinner backbones should be used. This design choice is also echoed by the experimental study in [21].

As explained by the kinematics in Sect. 4.2, bending of the distal segment is a 2-DoF motion. With the proximal segment, only two actuators are sufficient to drive the distal segment, no matter how many backbones are arranged.

Besides, the weight lifting experiments in [22] show that the payload capability of a continuum manipulator is also greatly affected by its torsional stability. Then two bellows, which can be easily bent but resist twisting as shown in Fig. 2, are used in the distal segment. The bellows' convolutions act as the spacer rings that prevent buckling of the backbones under compressive loads.

Actuation modularity is enabled by this dual continuum mechanism concept. The distal segment and the stem could be designed for different lengths, different diameters, and/or with different end effectors (e.g., grippers, scissors, cautery spatula, etc.). As far as the same proximal segment is used, the exchangeable effector could always be assembled into the actuation unit to bend the distal segment. The only modification required is to change the corresponding actuation parameters in the controller for different stems and/or distal segments.

Actuation of the gripper is also incorporated in the exchangeable effector as shown in Fig. 2(b). The gripper actuation rod is routed through a central channel and connected to a spring-loaded translating magnet. The magnet is pushed and pulled to close and open the gripper. The spring is used to avoid exerting excessive gripping force, while the magnet allows quick connection to the actuation unit.

The entire exchangeable effector only consists of mechanical components. It can be sterilized by emerging it in liquid agent such as glutaraldehyde and ortho-phthalaldehyde.

3.2 Actuation Unit

The actuation unit mainly consists of (i) one driving segment, (ii) two backbone driving assemblies, and (iii) a gripper driving assembly, as shown in Fig. 3. The actuation unit also includes casing and structural features that allow its attachment to a Denso manipulator.

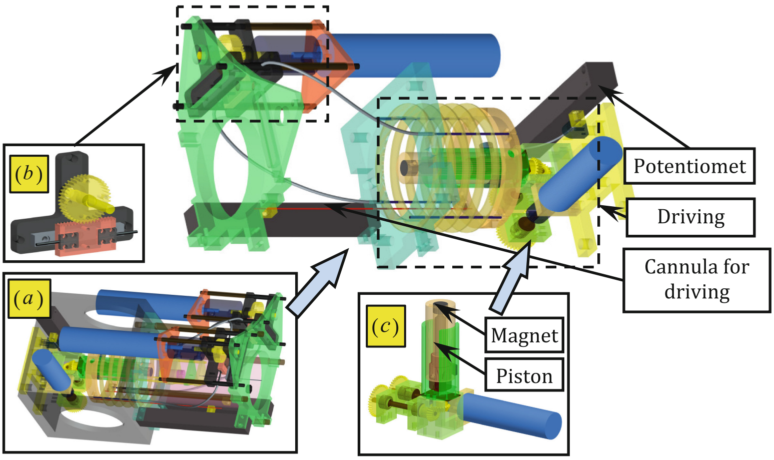

Fig. 3. Actuation unit of the SMARLT tool: (a) total assembly, (b) the backbone driving assembly, and (c) the gripper driving assembly

The driving segment is structurally similar to the one shown in Fig. 5(b), consisting of a base ring, several spacer rings, an end ring and four backbones made from ∅1 mm nitinol rods. It has matching geometries with the proximal segment in Fig. 2 so that the proximal segment can be securely assembled into the driving segment. Push-pull actuation of the driving backbones bends the driving and the proximal segments together so as to bend the distal segment. No matter how many backbones are arranged in the exchangeable effector, its actuation is always realized by the four driving backbones.

The backbone driving assembly pushes and pulls the driving backbones to bend the driving segment. According to the actuation kinematics in Eqs. (1) and (2), the two backbones that are 180° apart shall be pushed and pulled for the same amount at the same time.

As shown in Fig. 3(b), two driving backbones are connected to a rail-guided slider on which a rack is attached. The driving backbones are fixed to the end ring of the driving segment, routed through the guiding cannulae and the segment spacers respectively. A servomotor is connected to a pinion through a coupling to drive the rack to realize this push-pull actuation for the driving backbones.

A lead screw in the gripper driving assembly is driven by another servomotor through a gear train (including a pair of spur gears and a pair of bevel gears). A piston that is connected with the nut of the lead screw translates up and down. A magnet installed on the top of the piston allows quick connection to the translating magnet in the exchangeable effector. The attraction force between the magnets is big enough to pull the gripper open, while the piston pushes the magnets to close the gripper.

Potentiometers are installed in the gripper the backbone driving assemblies to sense the absolute positions of the lead screw and the driving backbones.

3.3 Control Infrastructure

The SMARLT's control infrastructure is set up so to allow teleoperation, which involves the control of the SMARLT tool and the Denso manipulator. A diagram of the control infrastructure is shown in Fig. 4.

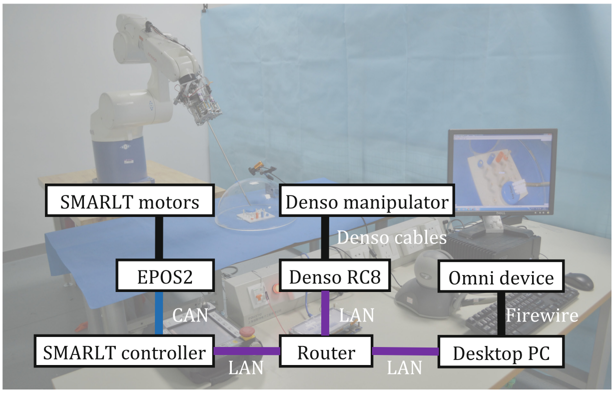

Fig. 4. Control infrastructure of the SMARLT and the Denso manipulator

A Phantom Omni device (Sensable Inc.) is connected to a desktop PC to acquire poses information. The SMARLT's central controller is an embedded system and it generates control reference signals for the SMARLT tool and the Denso manipulator according to the inputs from the Omni device and the inverse kinematics of the SMARLT and the Denso manipulator. The kinematics is detailed in Sect. 4.

The control references for the Denso manipulator are sent to the Denso RC8 controller (configured in a slave mode) via the LAN port using the UDP protocol so that the manipulator's joint references could be continuously updated.

The control signals for the SMARLT tool are sent to three Maxon EPOS2 24/2 digital controllers via the CAN bus. The EPOS2 controllers drive the servomotors in the actuation unit to drive the SMARLT tool.

The backbone driving assemblies use two Maxon A-max-22 motors. The gripper driving assembly uses one Maxon A-max-16 motor.

Three potentiometers in the actuation unit are read by the A/D ports of the EPOS2 controllers. The readings are sent back to the central controller via the CAN bus.

4 Kinematics Framework

As in Fig. 1, the continuum segment with a 2-DoF bending is incorporated in the SMARLT tool as a distal wrist. Kinematics of such a bending segment could be found in previous studies [7, 23, 24]. The segment's bending kinematics is summarized in Sect. 4.2 with the nomenclature and coordinates defined in Sect. 4.1.

The SMARLT tool is deployed and maneuvered by a manipulator (a 6-DoF Denso manipulator in this case) through a trocar. The Denso manipulator serves as a programmable RCM mechanism which positions and orients the SMARLT tool with respect to the trocar (the incision point, or the pivot point). The kinematics of the Denso manipulator system is presented in Sect. 4.3.

4.1 Nomenclature and Coordinates

The SMARLT is maneuvered by the 6-DoF Denso manipulator. Its distal segment is driven by the proximal segment that bends together with the driving segment. All the segments are structurally similar to the one shown in Fig. 5(b). Verified by the analytical and the experimental investigations, the segment's bent shapes could be approximated as circular arcs [7, 24]. The derived kinematics in Sect. 4.2 is based on this assumption.

Eleven coordinates are defined below with the nomenclature defined in Table 1 to describe the kinematics.

- *World Coordinate* $\{W\} \equiv \{\hat{\mathbf{x}}_W, \hat{\mathbf{y}}_W, \hat{\mathbf{z}}_W\}$ (or $\{D0\} \equiv \{\hat{\mathbf{x}}_{D0}, \hat{\mathbf{y}}_{D0}, \hat{\mathbf{z}}_{D0}\}$) is located at the base of the Denso manipulator.
- *Denso Coordinates* $\{Dj\} \equiv \{\hat{\mathbf{x}}_{Dj}, \hat{\mathbf{y}}_{Dj}, \hat{\mathbf{z}}_{Dj}\}$ (j = 1, 2, ⋯, 6) are assigned to the joint axes of the Denso manipulator according to the Denavit-Hartenberg rules.

- *Segment Base Coordinate* $\{S1\} \equiv \{\hat{\mathbf{x}}_{S1}, \hat{\mathbf{y}}_{S1}, \hat{\mathbf{z}}_{S1}\}$ is attached to the segment's base ring. The XY plane is aligned with the base ring with its origin at the center. $\{S1\}$ is translated from $\{D6\}$ by a distance h in the $\hat{\mathbf{z}}_{D6}$ direction. $\hat{\mathbf{x}}_{S1}$ points from the center to the 1st backbone. The backbones are numbered according to the definition of δ_i.
- *Segment Base Bending Coordinate* $\{S2\} \equiv \{\hat{\mathbf{x}}_{S2}, \hat{\mathbf{y}}_{S2}, \hat{\mathbf{z}}_{S2}\}$ shares its origin with $\{S1\}$ and has the segment bending in its XY plane.
- *Segment Tip Bending Coordinate* $\{S3\} \equiv \{\hat{\mathbf{x}}_{S3}, \hat{\mathbf{y}}_{S3}, \hat{\mathbf{z}}_{S3}\}$ is obtained from $\{S2\}$ by a rotation about $\hat{\mathbf{z}}_{S2}$ such that $\hat{\mathbf{x}}_{S3}$ becomes the backbone tangent at the end ring. Origin of $\{S3\}$ is at the center of the end ring.
- *Segment Tip Coordinate* $\{S4\} \equiv \{\hat{\mathbf{x}}_{S4}, \hat{\mathbf{y}}_{S4}, \hat{\mathbf{z}}_{S4}\}$ is fixed to the end ring. $\hat{\mathbf{x}}_{S4}$ points from the end ring center to the first backbone and $\hat{\mathbf{z}}_{S4}$ is normal to the end ring.

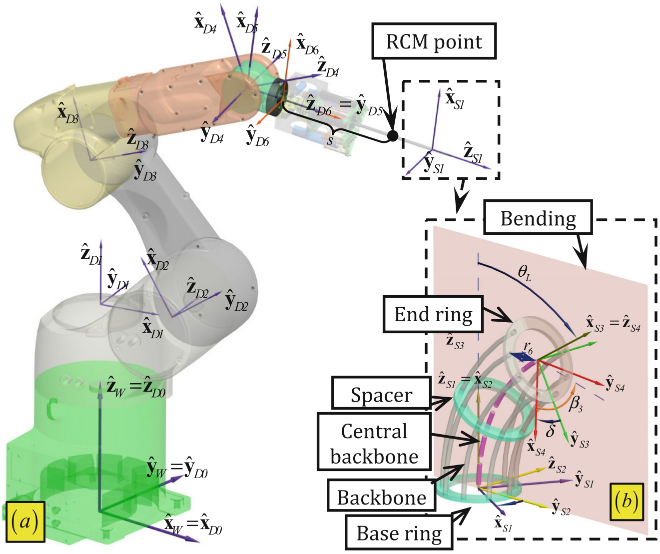

Fig. 5. Nomenclature and coordinates of the SMARLT-Denso system: (a) the Denso manipulator and (b) the bending segment

4.2 Kinematics of the Continuum Segment

As shown in Fig. 5(b), the backbones are pulled and pushed to bend the segment within the bending plane. The length and shape of the segment is indicated by a central backbone. According to previous investigations [7, 24], absence of the central backbone doesn't affect the bent shapes. In the case that the central backbone is removed to spare a lumen for passing through other components, a virtual central backbone still exists, governing the segment's length and shape.

The backbone shapes are approximated as circular arcs in planes parallel to the bending plane. The projection of one backbone on the bending plane has the same length as itself and is offset from the central backbone. The lengths of the central

Table 1. Nomenclature used in this paper

Symbol	Definition
j	Index of the Denso manipulator axes, $j = 1, 2, \cdots, 6$
φ_j	Joint variables of the Denso manipulator
$\mathbf{\Psi}_D$	$\mathbf{\Psi}_D \equiv [\varphi_1\ \varphi_2\ \cdots\ \varphi_6]^T$ is the manipulator's configuration vector
s	Distance along the SMARLT's stem from the $\{D6\}$ origin to the RCM point
h	Distance between the origins of $\{D6\}$ and $\{S1\}$ along the SMARLT's stem
i	Index of the segment backbones, $i = 1, 2, \cdots, m$
r_i	Distance from the virtual central backbone to the ith backbone
β_i	Division angle from the ith backbone to the 1st backbone; $\beta_1 = 0$ and β_i remain constant once the segment is built
L, L_i	Lengths of the central backbone and the ith backbone measured from the base ring to the end ring along the backbones
q_i	Push-pull actuation of the segment's ith backbone; $q_i \equiv L_i - L$
δ_i	A right-handed rotation angle about $\hat{\mathbf{z}}_{S1}$ from $\hat{\mathbf{y}}_{S2}$ to a ray passing through the central backbone and the ith backbone
δ	$\delta \equiv \delta_1$ and $\delta_i = \delta + \beta_i$
θ_L	The right-handed rotation angle from $\hat{\mathbf{x}}_{S2}$ to $\hat{\mathbf{x}}_{S3}$
$\mathbf{\Psi}_S$	$\mathbf{\Psi}_S \equiv [\theta_L\ \delta]^T$ is the segment's configuration vector
$\mathbf{\Psi}$	$\mathbf{\Psi} \equiv [\mathbf{\Psi}_D^T\ \mathbf{\Psi}_S^T]^T$ is the configuration vector of the entire system
${}^{S1}\mathbf{p}_L$	Center position of the segment's end ring in $\{S1\}$
${}^{1}\mathbf{R}_2$	Coordinate transformation matrix from frame 2 to frame 1
${}^{1}\mathbf{T}_2$	Homogeneous transformation matrix from frame 2 to frame 1

backbone and the ith backbone are related as in (1), as well as the backbone actuation, according to the definition of q_i.

$$\begin{cases} L_i = L - r_i\theta_L\cos(\delta + \beta_i) \\ q_i = -r_i\theta_L\cos(\delta + \beta_i) \end{cases} \tag{1}$$

In order to bend the segment to a configuration specified by $\mathbf{\Psi}_s$, each backbone should be pushed or pulled according to (1). When many thin backbones are used in the distal segment of the SMARLT's exchangeable effector for (i) enhanced reliability and (ii) increased payload capability, it is more effective to use the proximal segment to actuate the distal segment since the bending possesses 2 DoFs.

The backbones arrangements (specified by r_i and β_i) could be arbitrary but should be similar and scaled in the distal and the proximal segments. This means $(r_i)_{\text{proximal}} = (\kappa r_i)_{\text{distal}}$ as well as $(\beta_i)_{\text{proximal}} = (\beta_i)_{\text{distal}}$. Then a bending of θ_L and δ on the distal segment requires a bending of θ_L/κ and $\delta + \pi$ on the proximal segment. The driving segment has the same configuration as the proximal segment. Then the four driving backbones should be pushed and pulled according to (2) with the corresponding bent configuration variables (θ_L/κ and $\delta + \pi$) and the structural parameters listed in Table 2.

$$\begin{cases} q_1 = -(r_i)_{driving}\frac{\theta_L}{\kappa}\cos(\delta+\pi) = -q_3 \\ q_2 = -(r_i)_{driving}\frac{\theta_L}{\kappa}\cos\left(\delta+\frac{3\pi}{2}\right) = -q_4 \end{cases}, \ \kappa = \frac{(r_i)_{proximal}}{(r_i)_{distal}} \tag{2}$$

Table 2. Structural parameters of the SMARLT-Denso system

Denavit-Hartenberg parameters of the Denso manipulator				
No.	α_{i-1}	a_{i-1}	d_i	φ_i
1	0	0	473mm	φ_1
2	-π/2	180mm	0	$\varphi_2-\pi/2$
3	0	385mm	0	φ_3
4	-π/2	100mm	445mm	φ_4
5	π/2	0	0	φ_5
6	-π/2	0	90mm	φ_6

Distal segment	
r_i = 2.5mm	L = 40mm
Proximal segment	
r_i = 24mm	L = 35mm
Driving segment	
r_i = 30mm	L = 35mm
β_i = 0, π/2, π, 3π/2	
Translation	h = 580mm
Gripper tip	g = 15mm

The distal segment bends into circular arcs. Center position of the end ring is written as follows.

$$^{S1}\mathbf{p}_L = \frac{L}{\theta_L}\left[\cos\delta(1-\cos\theta_L) \quad \sin\delta(\cos\theta_L - 1) \quad \sin\ \theta_L\right]^T \tag{3}$$

Where $^{S1}\mathbf{p}_L = [0 \quad 0 \quad L]^T$ when $\theta_L \to 0$.

Transformation matrix $^{S1}\mathbf{R}_{S4}$ relates $\{S4\}$ to $\{S1\}$

$$^{S1}\mathbf{R}_{S4} = {}^{S1}\mathbf{R}_{S2}{}^{S2}\mathbf{R}_{S3}{}^{S3}\mathbf{R}_{S4} \tag{4}$$

Where $^{S1}\mathbf{R}_{S2} = \begin{bmatrix} 0 & \cos\delta & \sin\delta \\ 0 & -\sin\delta & \cos\delta \\ 1 & 0 & 0 \end{bmatrix}$, $^{S2}\mathbf{R}_{S3} = \begin{bmatrix} \cos\theta_L & -\sin\theta_L & 0 \\ \sin\theta_L & \cos\theta_L & 0 \\ 0 & 0 & 1 \end{bmatrix}$, and $^{S3}\mathbf{R}_{S4} = \begin{bmatrix} 0 & 0 & 1 \\ \cos\delta & -\sin\delta & 0 \\ \sin\delta & \cos\delta & 0 \end{bmatrix}$.

The segment's instantaneous kinematics (Jacobian) from the segment configuration space to the task space for the center of the end ring is as follows.

$$^{S1}\dot{\mathbf{x}} = \mathbf{J}_S\,\dot{\boldsymbol{\psi}}_S = \begin{bmatrix} \mathbf{J}_{\mathbf{v}S} \\ \mathbf{J}_{\boldsymbol{\omega}S} \end{bmatrix}\dot{\boldsymbol{\psi}}_S. \tag{5}$$

Where $^{S1}\mathbf{v} = \mathbf{J}_{\mathbf{v}S}\dot{\boldsymbol{\psi}}_S$ and $^{S1}\boldsymbol{\omega} = \mathbf{J}_{\boldsymbol{\omega}S}\dot{\boldsymbol{\psi}}_S$

$$\mathbf{J}_{\mathbf{v}S} = L\begin{bmatrix} \cos\,\delta\left(\frac{\cos\theta_L-1}{\theta_L^2}+\frac{\sin\,\theta_L}{\theta_L}\right) & \frac{\sin\,\delta}{\theta_L}(\cos\theta_L-1) \\ \sin\,\delta\left(\frac{1-\cos\theta_L}{\theta_L^2}-\frac{\sin\,\theta_L}{\theta_L}\right) & \frac{\cos\delta}{\theta_L}(\cos\theta_L-1) \\ -\frac{\sin\,\theta_L}{\theta_L^2}+\frac{\cos\theta_L}{\theta_L} & 0 \end{bmatrix} \tag{6}$$

$$\mathbf{J}_{\boldsymbol{\omega}S} = \begin{bmatrix} \sin\,\delta & \cos\delta\,\sin\,\theta_L \\ \cos\delta & -\sin\,\delta\,\sin\,\theta_L \\ 0 & \cos\theta_L-1 \end{bmatrix} \tag{7}$$

4.3 Kinematics of the Denso Manipulator

Kinematics of the Denso manipulator could be easily described following the Denavit-Hartenberg parameters listed in Table 2. A general form of the homogeneous transformation matrix is as follows.

$${}^{D(j-1)}\mathbf{T}_{Dj} = \begin{bmatrix} {}^{D(j-1)}\mathbf{R}_{Dj} & {}^{D(j-1)}\mathbf{p} \\ \mathbf{0}_{1\times3} & 1 \end{bmatrix}, \quad j=1,2,\cdots,6 \tag{8}$$

Where $${}^{D(j-1)}\mathbf{R}_{Dj} = \begin{bmatrix} \cos\varphi_j & -\sin\,\varphi_j & 0 \\ \sin\,\varphi_j\cos\alpha_{i-1} & \cos\varphi_j\cos\alpha_{i-1} & -\sin\,\alpha_{i-1} \\ \sin\,\varphi_j\sin\,\alpha_{i-1} & \cos\varphi_j\sin\,\alpha_{i-1} & \cos\alpha_{i-1} \end{bmatrix},$$ and ${}^{D(j-1)}\mathbf{p} = \begin{bmatrix} a_{j-1} & -d_j\sin\,\alpha_{i-1} & d_j\cos\alpha_{i-1} \end{bmatrix}^T$.

Jacobian matrix $\mathbf{J}_D$ of the Denso manipulator for the center of its distal flange could be derived in (9) to (11). The SMARLT tool is attached to the Denso manipulator through this flange.

$${}^{D0}\dot{\mathbf{x}} = \mathbf{J}_D\dot{\boldsymbol{\psi}}_D = \begin{bmatrix} \mathbf{J}_{\mathbf{v}D} \\ \mathbf{J}_{\boldsymbol{\omega}D} \end{bmatrix}\dot{\boldsymbol{\psi}}_D \tag{9}$$

Where ${}^{D0}\mathbf{v} = \mathbf{J}_{\mathbf{v}D}\dot{\boldsymbol{\psi}}_D$ and ${}^{D0}\boldsymbol{\omega} = \mathbf{J}_{\boldsymbol{\omega}D}\dot{\boldsymbol{\psi}}_D$, $\mathbf{J}_{\mathbf{v}D}, \mathbf{J}_{\boldsymbol{\omega}D} \in \Re^{3\times6}$

$$\begin{aligned} \mathbf{J}_{\mathbf{v}D} = \big[\, & {}^{D0}\hat{\mathbf{z}}_{\mathrm{D1}} \times {}^{D0}\mathbf{p}_{D1D6} \quad {}^{D0}\hat{\mathbf{z}}_{\mathrm{D2}} \times {}^{D0}\mathbf{p}_{D2D6} \quad {}^{D0}\hat{\mathbf{z}}_{\mathrm{D3}} \times {}^{D0}\mathbf{p}_{D3D6} \\ & \dot{\varphi}_4{}^{D0}\hat{\mathbf{z}}_{\mathrm{D4}} \times {}^{D0}\mathbf{p}_{D4D6} \quad \dot{\varphi}_5{}^{D0}\hat{\mathbf{z}}_{\mathrm{D5}} \times {}^{D0}\mathbf{p}_{D5D6} \quad \mathbf{0}\,\big] \end{aligned} \tag{10}$$

$$\mathbf{J}_{\boldsymbol{\omega}D} = \begin{bmatrix} {}^{D0}\hat{\mathbf{z}}_{D1} & {}^{D0}\hat{\mathbf{z}}_{D2} & {}^{D0}\hat{\mathbf{z}}_{D3} & {}^{D0}\hat{\mathbf{z}}_{D4} & {}^{D0}\hat{\mathbf{z}}_{D5} & {}^{D0}\hat{\mathbf{z}}_{D6} \end{bmatrix} \tag{11}$$

The 6th column of $\mathbf{J}_{\mathbf{v}D}$ is zero because the rotation of the 6th joint does not induce additional linear velocity at the center of the distal flange.

5 Conclusions and Future Work

This paper presents the design and preliminary development of a modular robotic laparoscopic tool for MIS: the SMARLT tool. A dual continuum mechanism concept is utilized in the design to ensure reliability as well as achieve enhanced distal dexterity, increased payload capability and actuation modularity under a simple construction. With the kinematics derived, SMARLT tool would be able to be maneuvered by a Denso manipulator to perform typical laparoscopic tasks under teleoperation.

The SMARLT could provide an alternative option to realize robotic laparoscopic surgeries. The future efforts will primarily focus on (i) the derivation of kinematics with constrained motions and teleoperation, (ii) the compensation of continuum segment actuation, (iii) the stiffness characterization and representative surgical tasks demonstration.

Acknowledgments. This work was supported in part by the National Natural Science Foundation of China (Grant No. 51435010 and Grant No. 51375295), and in part by the Shanghai Jiao Tong University Interdisciplinary Research Funds (Grant No. YG2013MS26).

References

1. Cuschieri, A.: Laparoscopic surgery: current status, issues future developments. Surgeon **3**(3), 125–138 (2005)
2. Taylor, R.H.: A perspective on medical robotics. Proc. IEEE **94**(9), 1652–1664 (2006)
3. Guthart, G.S., Salisbury, J.K.: The Intuitive^{TM} telesurgery system: overview and application. In: IEEE International Conference on Robotics and Automation (ICRA). San Francisco, CA (2000)
4. Guthart, G.: Annual report 2010, p. 108. Intuitive Surgical, Inc., Sunnyvale (2011)
5. Kanno, T., et al.: A forceps manipulator with flexible 4-DoF mechanism for laparoscopic surgery. IEEE-ASME Trans. Mechatron. **20**(3), 1170–1178 (2015)
6. Hong, M.B., Jo, Y.H.: Design of a novel 4-DoF wrist-type surgical instrument with enhanced rigidity and dexterity. IEEE-ASME Trans. Mechatron. **19**(2), 500–511 (2014)
7. Xu, K., Simaan, N.: An investigation of the intrinsic force sensing capabilities of continuum robots. IEEE Trans. Robot. **24**(3), 576–587 (2008)
8. Xu, K., Simaan, N.: Intrinsic wrench estimation and its performance index for multisegment continuum robots. IEEE Trans. Robot. **26**(3), 555–561 (2010)
9. He, C., et al.: Force sensing of multiple-DOF cable-driven instruments for minimally invasive robotic surgery. Int. J. Med. Robot. Comput. Assist. Surg. **10**(3), 314–324 (2014)
10. Leonard, S., et al.: Smart tissue anastomosis robot (STAR): a vision-guided robotics system for laparoscopic suturing. IEEE Trans. Biomed. Eng. **61**(4), 1305–1317 (2014)
11. Ma, R., et al.: Design and optimization of manipulator for laparoscopic minimally invasive surgical robotic system. In: 2012 International Conference on Mechatronics and Automation (ICMA). IEEE (2012)
12. Taylor, R.H., Stoianovici, D.: Medical robotics in computer-integrated surgery. IEEE Trans. Robot. Autom. **19**(5), 765–781 (2003)

13. Hadavand, M., et al.: A novel remote center of motion mechanism for the force-reflective master robot of haptic tele-surgery systems. Int. J. Med. Robot. Comput. Assist. Surg. **10**(2), 129–139 (2014)
14. Kuo, C.H., Dai, J.S.: Kinematics of a fully-decoupled remote center-of-motion parallel manipulator for minimally invasive surgery. J. Med. Devices-Trans. ASME **6**(2), 021008 (2012)
15. Nasseri, M.A., et al.: Virtual fixture control of a hybrid parallel-serial robot for assisting ophthalmic surgery: an experimental study. In: 2014 5th IEEE RAS & EMBS International Conference on Biomedical Robotics and Biomechatronics (BioRob), pp. 732–738 (2014)
16. Lopez, E., et al.: Implicit active constraints for robot-assisted arthroscopy. In: 2013 IEEE International Conference on Robotics and Automation (ICRA), pp. 5390–5395 (2013)
17. Dubrowski, A., et al.: Quantification of motion characteristics and forces applied to tissues during suturing. Am. J. Surg. **190**(1), 131–136 (2005)
18. Okamura, A.M.: Methods for haptic feedback in teleoperated robot-assisted surgery. Ind. Robot Int. J. **31**(6), 499–508 (2004)
19. Berg, D.R., et al.: Determination of surgical robot tool force requirements through tissue manipulation and suture force measurement. Trans. ASME-W-J. Med. Devices **5**(2), 027517 (2011)
20. Xu, K., Zhao, J., Fu, M.: Development of the SJTU unfoldable robotic system (SURS) for single port laparoscopy. IEEE/ASME Trans. Mechatron. **20**(5), 2133–2145 (2014)
21. Xu, K., Fu, M., Zhao, J.: An experimental kinestatic comparison between continuum manipulators with structural variations. In: IEEE International Conference on Robotics and Automation. HongKong (2014)
22. Zhao, J., et al.: An endoscopic continuum testbed for finalizing system characteristics of a surgical robot for NOTES procedures. In: IEEE/ASME International Conference on Advanced Intelligent Mechatronics (AIM), Wollongong, Australia, pp. 63–70 (2013)
23. Webster, R.J., Jones, B.A.: Design and kinematic modeling of constant curvature continuum robots: a review. Int. J. Robot. Res. **29**(13), 1661–1683 (2010)
24. Xu, K., Simaan, N.: Analytic formulation for the kinematics, statics and shape restoration of multibackbone continuum robots via elliptic integrals. J. Mech. Robot. **2**(1), 011006 (2010)